

Femtosecond broadband fluorescence upconversion spectroscopy: Improved setup and photometric correction

X.-X. Zhang, C. Würth, L. Zhao, U. Resch-Genger, N. P. Ernsting et al.

Citation: *Rev. Sci. Instrum.* **82**, 063108 (2011); doi: 10.1063/1.3597674

View online: <http://dx.doi.org/10.1063/1.3597674>

View Table of Contents: <http://rsi.aip.org/resource/1/RSINAK/v82/i6>

Published by the [American Institute of Physics](http://www.aip.org).

Related Articles

Compact metal probes: A solution for atomic force microscopy based tip-enhanced Raman spectroscopy
Rev. Sci. Instrum. **83**, 123708 (2012)

Broadband photon-counting Raman spectroscopy in short optical waveguides
Appl. Phys. Lett. **101**, 211110 (2012)

Antenna-enhanced infrared near-field nanospectroscopy of a polymer
Appl. Phys. Lett. **101**, 193105 (2012)

Comparisons of 2D IR measured spectral diffusion in rotating frames using pulse shaping and in the stationary frame using the standard method
J. Chem. Phys. **137**, 184201 (2012)

Constant current etching of gold tips suitable for tip-enhanced Raman spectroscopy
Rev. Sci. Instrum. **83**, 103708 (2012)

Additional information on *Rev. Sci. Instrum.*


Journal Homepage: <http://rsi.aip.org>

Journal Information: http://rsi.aip.org/about/about_the_journal


Top downloads: http://rsi.aip.org/features/most_downloaded

Information for Authors: <http://rsi.aip.org/authors>

ADVERTISEMENT



**Does your research require low temperatures? Contact Janis today.
Our engineers will assist you in choosing the best system for your application.**



10 mK to 800 K **LHe/LN₂ Cryostats**
Cryocoolers **Magnet Systems**
Dilution Refrigerator Systems
Micro-manipulated Probe Stations

sales@janis.com **www.janis.com**
Click to view our product web page.

Femtosecond broadband fluorescence upconversion spectroscopy: Improved setup and photometric correction

X.-X. Zhang,^{1,3} C. Würth,² L. Zhao,¹ U. Resch-Genger,² N. P. Ernsting,^{3,a)} and M. Sajadi^{3,b)}

¹Photronics Center, College of Physical Science, Nankai University, Tianjin, China

²Federal Institute for Materials Research and Testing, Berlin, Germany

³Department of Chemistry, Humboldt Universität zu Berlin, Germany

(Received 2 March 2011; accepted 16 May 2011; published online 17 June 2011)

A setup for fluorescence upconversion spectroscopy (FLUPS) is described which has 80 fs temporal response (fwhm) for emission in the spectral range 425–750 nm. Broadband phase matching is achieved with tilted gate pulses at 1340 nm. Background from harmonics of the gate pulse is removed and sensitivity increased compared to previous designs. Photometric calibration of the upconversion process is performed with a set of fluorescent dyes. For Coumarin 153 in methanol the peak position, bandwidth, and asymmetry depending on delay time are reported. © 2011 American Institute of Physics. [doi:10.1063/1.3597674]

I. INTRODUCTION

Time-resolved fluorescence upconversion was first reported by Mahr and Hirsch in 1975.¹ A chromophore in solution is excited with short optical pulses, and its emission at wavelength λ_F is mixed with short gate pulses at λ_G in a nonlinear optical (NLO) crystal. Sum-frequency generation occurs at a well-defined crystal orientation when phase matching conditions are met. In this case upconverted light at λ_U is generated and detected. By plotting the intensity $I_U(t)$ as function of time delay t between pump and gate pulses, a “kinetic trace” of the fluorescence at the chosen wavelength is obtained. This kind of measurement is well suited to measure short excited-state lifetimes. In step with advances in ultrafast laser technology, the accuracy improved steadily and the spectral scope widened. Representative examples and some milestones on this way are given in Refs. 2–27.

Spectral evolution of the fluorescence may indicate a photochemical reaction or a photophysical process in the excited singlet state; examples are *cis/trans* isomerization,^{4,20,27} proton-transfer^{10–14,23} or electron-transfer,^{8,21,24} and dynamic solvation.^{3,5,9,16,17,22,37} To understand such processes one must obtain not only an amplitude at various delay times t , but also the shape of the entire fluorescence quantum distribution $F(t, \lambda_F)$. This is usually achieved by recording 10–20 kinetic traces $I_U(t)$, corresponding to different λ_F which cover the emission region. The results are depicted schematically in Fig. 1. Because the crystal is rotated between recording kinetic traces, their relative amplitudes are usually not defined during measurement. Instead, amplitude scaling is performed afterwards with the help of additional information such as the steady-state emission spectrum of the compound under investigation. Spectral reconstruction then yields the desired transient emission spectra.^{9,28,29}

For photometric accuracy it is better to record the contiguous emission spectrum for any given delay time. The order of measurement should therefore be inverted. Whereas before, λ_F is kept fixed while t is scanned, now instead, for every fixed delay the fluorescence wavelength is scanned. By this procedure, intensities for adjacent emission wavelengths are compared directly, allowing a more accurate correction of the apparatus response which may strongly depend on wavelength. Coverage of the fluorophore’s emission region has been realized in various ways. The methods are: (i) rotation of the NLO crystal while synchronously scanning the detection monochromator,^{17,19,30} (ii) wobbling the crystal while detecting with a spectrograph,³¹ and (iii) simultaneous phase matching across a broad spectral range followed by multiplex detection.^{32–34}

Broadband fluorescence upconversion spectroscopy (FLUPS), developed systematically in our laboratory along (iii),^{32–34} has similarities with ultrafast pulse generation by nonlinear-optical parametric amplification. Indeed, parametric amplification offers an alternative route to time-resolved fluorescence spectra,^{35,36} but so far the band shape could not be recorded accurately with this method. This renders FLUPS more promising. For gating we use near-infrared pulses at $\lambda_G \approx 1340$ nm. Tilting of the gate pulses³⁴ turned out to be crucial to achieve a time resolution (fwhm of instrument response) of 80 fs. However, two deficiencies remained: first, background due to direct fluorescence, and second, signal from the third-harmonic of the gate pulse which blocked the range $\lambda_F > 600$ nm. To overcome these drawbacks, we designed an improved setup which is easier to align, more sensitive, and – most importantly – background free. This enables photometric correction of broadband sum-frequency for emission wavelengths $\lambda_F = 425 - 750$ nm.

In addition to instrument characterization, the increasing collaboration between laboratories triggers the need for a dynamic fluorescence standard. The dynamics of methanol is a case in point. For such measurements one observes the dynamic solvation of a polar molecular probe, for exam-

a)Electronic mail: nernst@chemie.hu-berlin.de.

b)Electronic mail: sajadimo@chemie.hu-berlin.de.

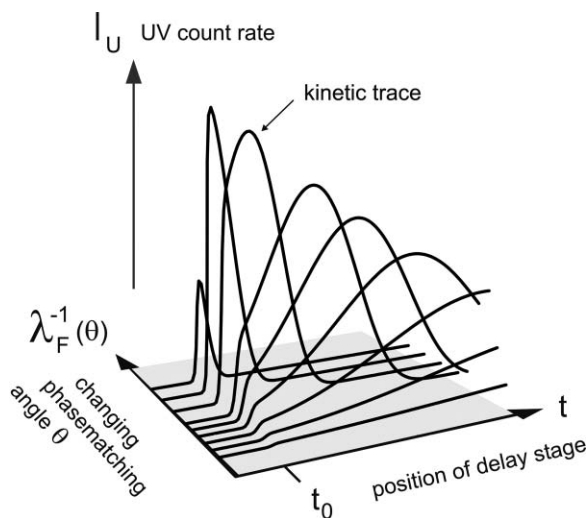


FIG. 1. With conventional fluorescence-upconversion, the emission wavelength λ_F is kept fixed while the time delay t is scanned, resulting in a kinetic trace. Relative amplitudes are obtained with the help of the stationary fluorescence spectrum. Transient spectra are constructed from 10–20 traces.

ple, Coumarin 153 (C153). Figure 2 shows its absorption and stationary emission spectra. An estimate of the initial fluorescence band, after vibrational relaxation but before solvation,³⁸ is shown as a dashed line. The methanol dynamics is assumed to be reflected by the spectral position $\tilde{\nu}(t)$ of the fluorescence band (peak position or first moment) as a function of time. Polar solvation of C153 has been the subject of numerous experimental^{9,17,34,37–40} and theoretical^{41,42} studies. In Fig. 3 we compare the $\tilde{\nu}(t)$ curves for methanol reported by different groups.^{9,17,37,40,43} To facilitate the comparison, curves $C(t) \propto \tilde{\nu}(t) - \tilde{\nu}(\infty)$ are shown that are scaled to a common value⁹ at $t = 0.20$ ps. At this time the fluorescence spectrum should have been fully time-resolved in all

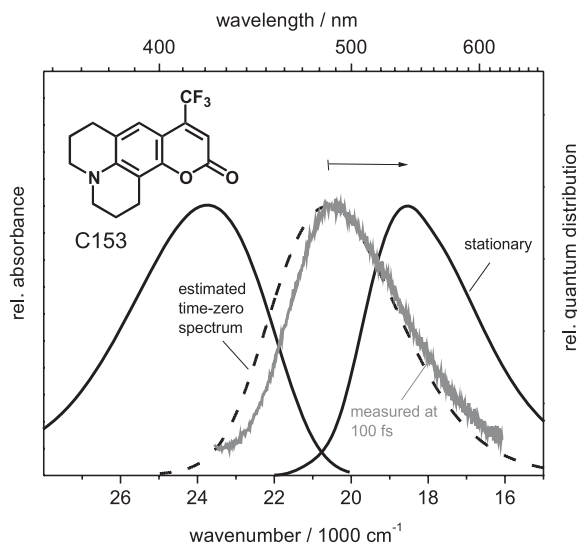


FIG. 2. Absorption and fluorescence spectra (quantum distributions over energy) of Coumarin 153 (inset) in methanol. (Dashed) Time-zero estimate,³⁸ (gray) transient fluorescence spectrum at 0.1 ps of this work. The time-dependent Stokes shift of fluorescence is indicated by a horizontal arrow.

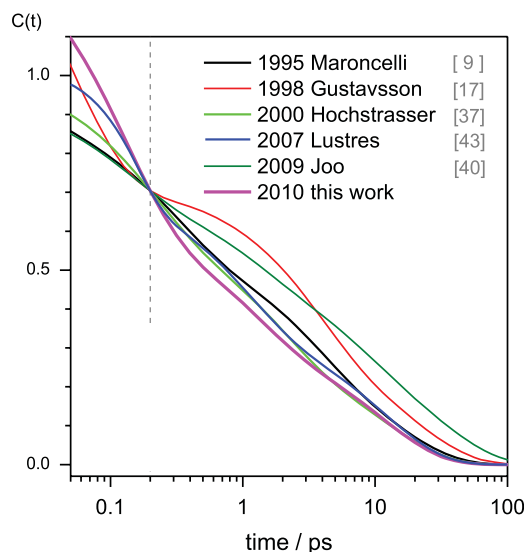


FIG. 3. (Color online) Reports of the dynamic Stokes shift of C153 fluorescence in methanol: The “spectral relaxation functions” $C(t)$ are set to a common value 0.704 at $t = 0.20$ ps¹⁰ when spectra were fully time-resolved. The relative variance at 10 ps, for example, is $\sim 30\%$, limiting the accuracy of $C(t)$ measurements. Reports of the time-dependent fluorescence bandwidth and asymmetry^{10,35,40} vary more strongly.

cases. The variances between these results are notable, considering that C153 is the best-studied polarity probe. Similar discrepancies must be expected when results from different laboratories are combined to support a microscopic model for the spectral relaxation, thus limiting the significance of the model.

Why are the $C(t)$ curves of Fig. 3 so different? When measurements of transient absorption are used^{37,43} the main problem is the extraction of the band for stimulated emission. Conventional upconversion methodology,^{9,40} whereby spectra are reconstructed from kinetic traces, suffers from a lack of stationary calibration light on the blue side, in combination with (relatively) sparse spectral coverage. The latter problem is solved by synchronous wavelength scanning of the crystal angle and detection monochromator, before the next delay time is accessed.¹⁷ In this case geometrical instabilities might play a role.

Broadband upconversion with a fixed crystal angle, by comparison, simultaneously monitors a range of frequencies and therefore needs less integration time to achieve the same signal/noise; also it allows better control of the geometry. Using this method, we quantify the C153 fluorescence in methanol in terms of peak position, bandwidth, and asymmetry depending on delay time.

II. OPTIMIZED OPTICAL SETUP FOR FS BROADBAND FLUORESCENCE UPCONVERSION

A. Gate pulse compression and tilting

The fs fluorometer is shown in Fig. 4. A Ti:sapphire laser (Femtolasers *sPro*) provides 30 fs, 500 μ J pulses at 800 nm (500 Hz repetition rate). This beam is split with a 6:1 ratio. Pulses of 430 μ J drive a traveling-wave optical parametric

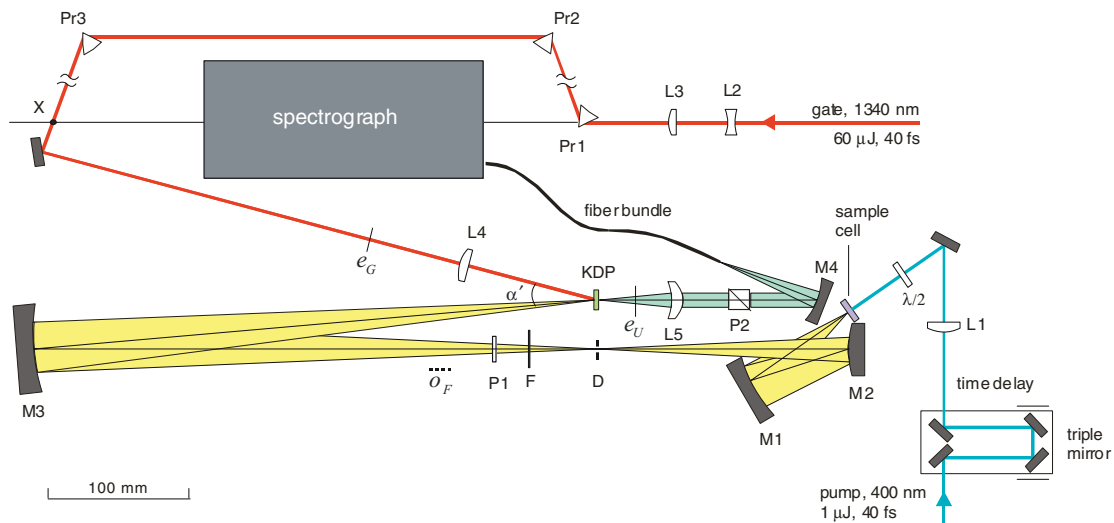


FIG. 4. (Color online) Setup for broadband fluorescence upconversion spectroscopy. Pr – prisms; M_{1-4} – spherical mirrors; L – lenses; P – polarizers.

amplifier of superfluorescence (TOPAS, Lightconversion) which delivers $60 \mu\text{J}$, 1340 nm pulses in horizontal polarization, to be used for optical gating. The beam is widened and collimated by a telescope L_2/L_3 with $-50\text{-mm}/+200\text{-mm}$ lenses. All lenses in the gate path have antireflective coating at 1300 nm . For compression and subsequent tilting a combination of three prisms Pr_{1-3} (Schott SF50, apex angle 55.5°) is used. The fourth prism of a normal compressor would be located at point X.⁴⁴ The tilt angle $\Phi = 3.55^\circ$ of the pulse front at X (due to the action of prism Pr_3) is calculated from Eq. (1) of Ref. 34. X is imaged by a thin lens L_4 ($f = 140 \text{ mm}$) onto the potassium dihydrogen phosphate (KDP) crystal, whereby the tilt angle is leveraged to 20° at the crystal. Fine adjustment of the crystal-lens distance, and hence the tilt, is done simply by observing the generated sum frequency (from the pump laser) on a white piece of paper. When aligned properly, the upconverted light appears and disappears at the same location on the paper when

the time difference between pump and gate pulses is varied, otherwise it moves across the wider upconversion pattern.

B. Fluorescence excitation, collection, and imaging

For optical pumping, the rest of the fundamental light is frequency doubled to 400 nm pulses which have 40 fs fwhm after compression. Their polarization is set with a $\lambda/2$ plate. After passing a triple mirror on a variable delay stage, attenuated pump pulses ($\sim 1 \mu\text{J}$) are focused by a thin lens L_1 ($f = 200 \text{ mm}$, fused silica, *f.s.*) onto the sample cell, to a spot diameter $\leq 0.1 \text{ mm}$. To obtain an optical image with the subsequent collection optics, the cell is made as thin as possible for a given solution (*f.s.* windows, 0.2 mm thick, are typically spaced $0.2\text{--}0.3 \text{ mm}$ apart). The sample solution is pumped through the cell which can also be oscillated perpendicular to the beam direction.

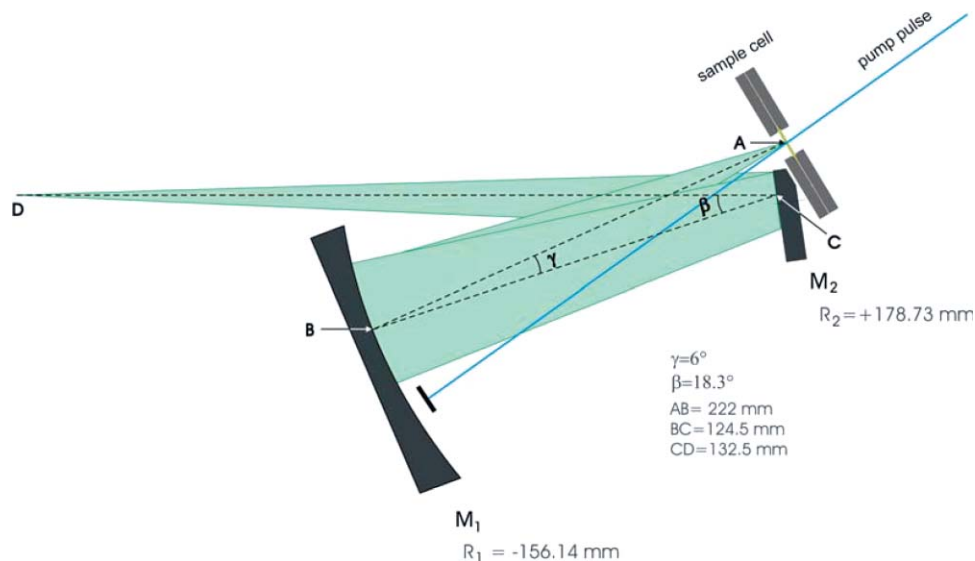


FIG. 5. (Color online) Off-axis Schwarzschild objective for fluorescence collection, allowing to oscillate the sample cell perpendicular to the pump beam.

An off-axis Schwarzschild objective (Fig. 5) refocuses the generated fluorescence with sevenfold magnification at intermediate position D. This arrangement provides more degrees-of-freedom to the sample cell compared to the axial geometry.³⁴ Fluorescence emitted from source A into the full angles 18° and 40° in horizontal and vertical planes, respectively, is collected by concave mirror M_1 , consistent with the acceptance angles for sum-frequency generation. The effective waist diameter at D is 0.6 mm, allowing to select vertical polarization by a miniature Glan polarizer here.^{45,46} For fluorescence wavelengths $\lambda_F \geq 420$ nm a wire-grid polarizer P_1 (Moxtec PPL04C, on $700 \mu\text{m}$ of Corning 1737F glass) is used instead. Pump scatter and low-frequency Raman signal are reduced with a long-pass edge filter (Schott GG420, 2 mm). The fluorescence from D is relayed 1:1 onto the KDP crystal by concave mirror M_3 ($R_3 = -400$ mm).

C. Sum-frequency generation

For sum-frequency generation we use a KDP crystal cut at $\theta_N = 65^\circ$, with the crystal axis in the horizontal plane. At first sight BBO might be considered superior due to its higher nonlinear susceptibility, but this advantage is more than cancelled by increased dispersion which limits broadband operation. The KDP crystal of thickness $L = 0.3$ mm has antireflection (AR) coating at 520 nm and 1300 nm on the input face, and at 360 nm on the output face (EKSMa). The central rays of the fluorescence and the gate beam form an external gating angle $\alpha' \approx 20^\circ$ at the crystal (internal angle $\alpha \approx 13^\circ$). Type II phase matching is chosen because it provides the broadest spectral window. Vertically polarized fluorescence at λ_F (o – ordinary in terms of crystal axes) interacts with horizontally polarized gate pulses at $\lambda_G = 1340$ nm (e – extraordinary), to generate horizontally polarized upconverted light at λ_U (e). Phase matching requires minimizing the wave vector mismatch $\Delta\vec{k} = \vec{k}_U(\theta_U) - \{\vec{k}_{oF}(\theta_U) + \vec{k}_{eG}(\theta_G)\}$ over a wide range of λ_F , for example 400–800 nm. The quantum efficiency of the upconversion process is⁴⁷

$$\eta_{\text{NLO}} = \frac{N_U(z=L)}{N_F(z=0)} = \frac{2^7 \pi^3 I_G(z=0)}{c^3} \times \left[\frac{\omega_U \omega_F d_{\text{eff}}^2}{n_e(\omega_U) n_o(\omega_F) n_e(\omega_G)} \right] \left[\frac{\sin(\Delta k L/2)}{\Delta k L/2} \right]^2 L^2. \quad (1)$$

Here, N is the photon flux, is the intensity of the gate light, L is the crystal thickness, n_{eo} are the pertinent refractive indices, d_{eff} is the effective nonlinear susceptibility, and ω_{FGU} are the angular frequencies. Figure 6 shows mismatch curves $\Delta\vec{k}(\lambda_F)$ for different cut angles θ_N (Note that Eq. (11) of Ref. 34 contains a sign error which has been corrected in Fig. 6(a)). The efficiency curve $\eta(\lambda_F)$ depends sensitively on thickness L (Fig. 6(b)) and external beam angle α' (Fig. 6(c)). A range of angles contributes to the upconverted signal, resulting in the measured efficiency curve (Fig. 6(d)) which was obtained upon photometric correction. Calculating the group velocity mismatch (between gate and fluorescence

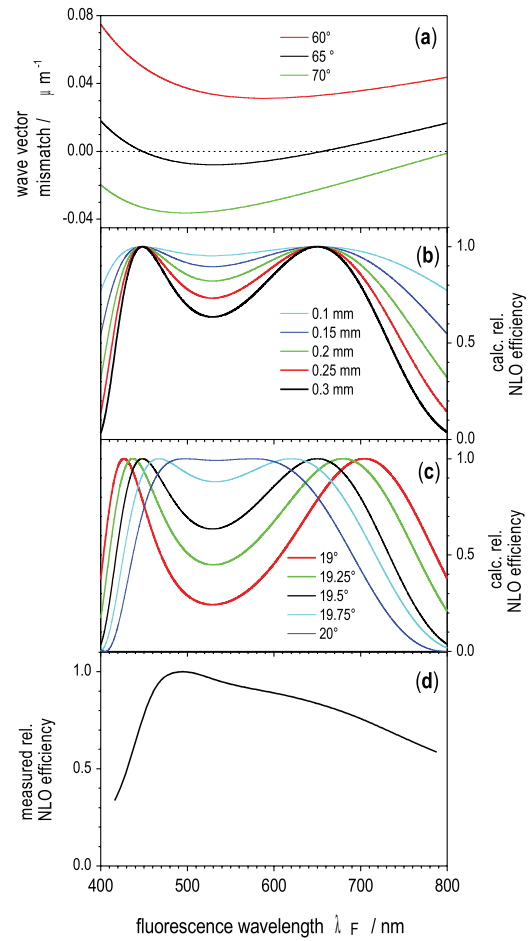


FIG. 6. (Color online) (a) Phase matching curve for type II sum-frequency generation, for three cut angles θ_N of a KDP crystal with gate pulses at 1340 nm. Gate and fluorescence beams have external angle $\alpha' = 19.5^\circ$ between them. (b) Relative conversion efficiency $[\sin(\Delta k L/2)/(\Delta k L/2)]^2 L^2$ for different crystal thicknesses ($\theta_N = 65^\circ$, $\alpha' = 19.5^\circ$). (c) Efficiency when varying the angle α' , for a crystal of 0.3 mm thickness cut at 65° , with gate wavelength of 1340 nm. (d) Experimental NLO efficiency, i.e., $1/\bar{c}(p)$ of Fig. 8, divided by the quantum efficiency of the UV detection system.

light, in the fluorescence direction) for these angles, we find that their passage times differ by < 20 fs.

D. UV collection, dispersion, and detection

The upconverted signal is collimated by a meniscus lens L_5 ($f = +50$ mm, *f.s.*, AR-coated for the UV). It is then passed through a Glan polarizer P_2 ($10 \times 10 \times 10$ mm³, Halle Nachfl.) to suppress direct fluorescence, pump scatter, and gate harmonics. The concave mirror M_4 ($R_4 = -70$ mm) collects and focuses the signal light on the entrance of a fiber bundle. The bundle (CeramOptec) consists of 30 *f.s.* fibers of 100 μm diameter, compacted into a round shape (0.6 mm diameter) at the input and into a slit (0.1×3.3 mm) at the spectrograph. This UV geometry allows suppressing the background signal which hampered the previous setup for $\lambda_F > 600$ nm due to better use of the Glan polarizer. An important aspect of the geometry is the large input angle α' .

The spectrograph employs a ruled plane grating (Newport 53–080R) in a Czerny–Turner mount. Photon loss to unused orders is reduced, and the UV efficiency is maximized by the choice of blaze angle. The linear wavelength calibration $\lambda_U(p)$ as function of pixel number p is obtained with a mercury lamp. The spectral range $\lambda_U = 307 - 478$ nm (corresponding to $\lambda_F = 400 - 750$ nm) is mapped onto a spectrum 21 mm wide. It is recorded with a CCD camera (Andor DV420-BU, 25 μ m pixel width). For example, photons at $\lambda_U = 374$ nm ($\lambda_F = 522$ nm) are binned into a 14.5 cm^{-1} energy segment. The resolution of the spectrograph is 50 cm^{-1} (fwhm of spectral instrument response).

Using the dye C153 in methanol as described below, we measure a count rate of $\sim 100 \text{ s}^{-1}$ at long delay times. (The sensitivity is ~ 1.5 -fold higher than in Ref. 34 because of the new collection optics, but signal/noise is increased by a factor 3 because background has been removed.) The integration time is 1 s. For a time scan, the background is first recorded four times at negative delay, averaged, and smoothed. This background is subsequently subtracted from each recorded spectrum while the delay is scanned. Results from 16 time scans are individually corrected for cosmic spikes and then averaged.

III. CORRECTION PROCEDURES

A. Photometric correction

The correction is performed with the “standard” dyes BBOT (2,5-bis[5-*tert*-butylbenzoxazolyl(2)]thiophene, CAS 7128–64-5), Coumarin 6H (58336–35-9), Coumarin 153 (53518–18-6), and DCM (51325–91-8) in methanol. The absorbance at the pump wavelength is set to 0.4 in order to limit the inner filter effect. (Steady-state absorption spectra are shown in the supplementary material.⁵³ Note that also excited-state absorption affects the fluorescence signal³³.) The λ_F regions which were used to correct the spectral responsivity of the setup are 425–630, 470–690, and 600–750 nm for the last three dyes.

The development in Ref. 34 is summarized here for completeness. Consider an upconversion experiment with a standard dye whereby a total number $\Sigma^{(U)}$ of counts in the UV is registered. The time delay is chosen to be 250 ps so that nuclear relaxation in methanol has ceased. Actually one records the “technical” signal- or count-distribution over pixels p , $s^{(U)}(p) \equiv (\partial \Sigma^{(U)} / \partial p)(p)$. This is to be compared with the “molecular” stationary distribution of $\Phi^{(F)}$ fluorescence photons over wavenumbers in the visible, $f^{(F)}(\tilde{\nu}_F) \equiv (\partial \Phi^{(F)} / \partial \tilde{\nu}_F)(\tilde{\nu}_F)$. The latter is conveniently provided as a sum of lognormal functions:⁴⁸

$$\log \text{norm}(\tilde{\nu}_F) = h \exp \left\{ -\ln 2 \left(\frac{\ln [1 + 2\gamma(\tilde{\nu}_F - \tilde{\nu}_0)/\Delta]}{\gamma} \right)^2 \right\}. \quad (2)$$

Optimal values for peak wavenumber $\tilde{\nu}_0$ [cm^{-1}], width Δ [cm^{-1}], asymmetry γ [–], and amplitude h from conventional fluorescence measurements are collected in Table I. In

TABLE I. Lognormal parameters (Eq. (2)) for the fluorescence quantum distributions over wavenumbers, $f^{(F)}(\tilde{\nu}_F)$, in methanol.

	$\tilde{\nu}_0(\text{cm}^{-1})$	$\Delta(\text{cm}^{-1})$	γ	h
BBOT	24 457	952	0.0303	0.4153
	23 859	2126	0.001	0.1797
	22 975	1517	0.0564	0.8736
	21 532	1599	–0.3423	0.6292
	19 826	1989	–0.567	0.1546
	18 600	9937	–0.7929	0.0158
C6H	23 200	886	0	0.0255
	21 000	774	0.087	0.0203
	20 717	2950	–0.308	0.9774
	15 500	3186	0	0.0499
C153	20 481	1601	–0.218	0.0724
	18 519	2947	–0.402	0.9913
	16 537	2884	–0.781	0.0904
DCM	15 829	2388	–0.056	1.0000

addition to the spectrograph calibration $\lambda_U(p)$ we also need the relationship

$$\lambda_F(p) = \frac{\lambda_G \lambda_U(p)}{\lambda_G - \lambda_U(p)}, \quad (3)$$

which involves the gate wavelength λ_G . Figure 7 shows several upconversion spectra which are obtained when dye fluorescence is passed through narrowband interference filters as indicated. For any such combination, the peak wavelength $\lambda_{F\text{max}}$ of the transmitted fluorescence light is known from stationary measurements, and the corresponding pixel number p_{max} is obtained from the figure. Optimization gives $\lambda_G = 1340 \pm 4$ nm (see supplementary material).⁵³

Next, the stationary distribution $f^{(F)}(\tilde{\nu}_F)$ is transformed into an equivalent distribution of “upconverted” fluorescence

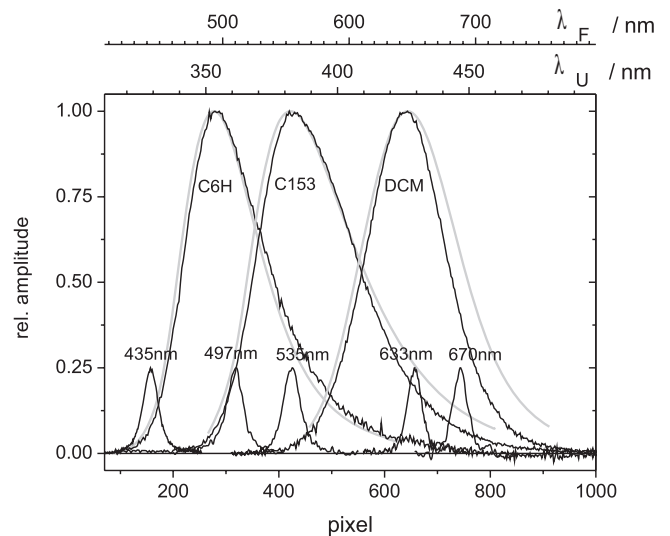


FIG. 7. Experimental *UV-count* distributions $s^{(U)}(p)$ over pixels (black lines) from fluorescence upconversion measurements of the dyes C6H, C153, and DCM in methanol at 250 ps delay time (for BBOT see Fig. 9). Also shown are the count distributions when the fluorescence has been passed through interference filters which are centered at the indicated wavelengths. For comparison, the expected *UV-photon* distributions $f^{(U)}(p)$ (gray lines) were inferred from stationary fluorescence measurements.

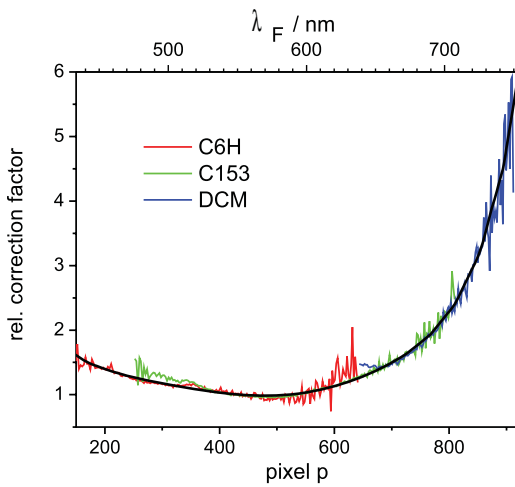


FIG. 8. (Color online) Photometric correction curves $c_i(p)$ (see text for definition and use) obtained by comparing the count distributions in Fig. 7 with the expected photon distributions. The black line $\bar{c}(p)$ is a polynomial fit.

photons over pixels:

$$f^{(U)}(p) \equiv \left(\frac{\partial \Phi^{(U)}}{\partial p} \right) (p) \propto \lambda_U^{-2} f^{(F)}(\tilde{\nu}_F) \cdot \left(\frac{\partial \lambda_U}{\partial p} \right) \quad (4)$$

with $\lambda_U(p)$ and $\tilde{\nu}_F(p)$.

The two types of spectra, $s^{(U)}(p)$ and $f^{(U)}(p)$, are shown in Fig. 7 (black and gray lines, respectively) for each standard dye. The correction function is then

$$c(p) \propto f^{(U)}(p)/s^{(U)}(p). \quad (5)$$

Figure 8 shows the $c(p)$ segments which correspond to the dyes in Fig. 7. They are scaled so that their rms differences are minimized, and a smooth fit provides the final correction curve $\bar{c}(p)$.

The correction function $\bar{c}(p)$ is used as follows. Pointwise multiplication of a measured, technical count distribution $s^{(U)}(p)$ with $\bar{c}(p)$ gives the distribution $f^{(U)}(p)$ of upconverted UV photons. To obtain the fluorescence distribution over fluorescence wavenumbers, $f^{(U)}(p)\lambda_U^2(p)$ is plotted against $10^7/\lambda_F(p)$. To obtain the fluorescence distribution over fluorescence wavelengths, $f^{(U)}(p)\lambda_U^2(p)/\lambda_F^2(p)$ is plotted against $\lambda_F(p)$. (Here it was assumed that λ_U is linear in p .)

B. Group delay correction

Before gating, fluorescence passes the exit window of the sample cell, polarizer, and glass filter. These optical elements cause group velocity dispersion, which is measured by gating a white-light continuum. The latter is generated by focusing 10 μ J pump pulses with a thin lens ($f = 100$ mm *f.s.*) into the cell containing pure methanol. For each pixel the transient signal is fitted with a temporal Gaussian function, and the dispersion curve is obtained by taking the peak position of the fit as a function of pixel number. The temporal response is given by the fwhm ≈ 80 fs of the Gaussian fits. To check the accuracy of the time correction obtained from continuum measurement,

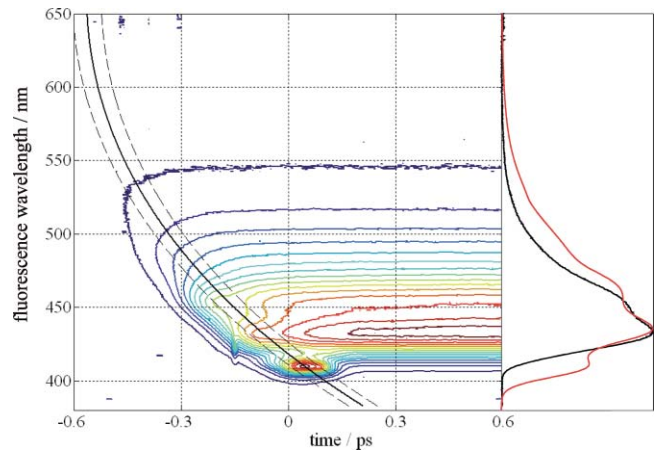


FIG. 9. (Color online) *Left*: The curve for time-zero as function of emission wavelength is plotted on top of the transient fluorescence of BBOT in methanol. The band ± 40 fs indicates the width (fwhm) of the temporal apparatus function. Following red-edge excitation at 400 nm, spectral broadening is observed during the first 0.2 ps. *Right*: The measured count distribution over wavelengths at late delay time (black line), compared to the stationary photon distribution (gray).

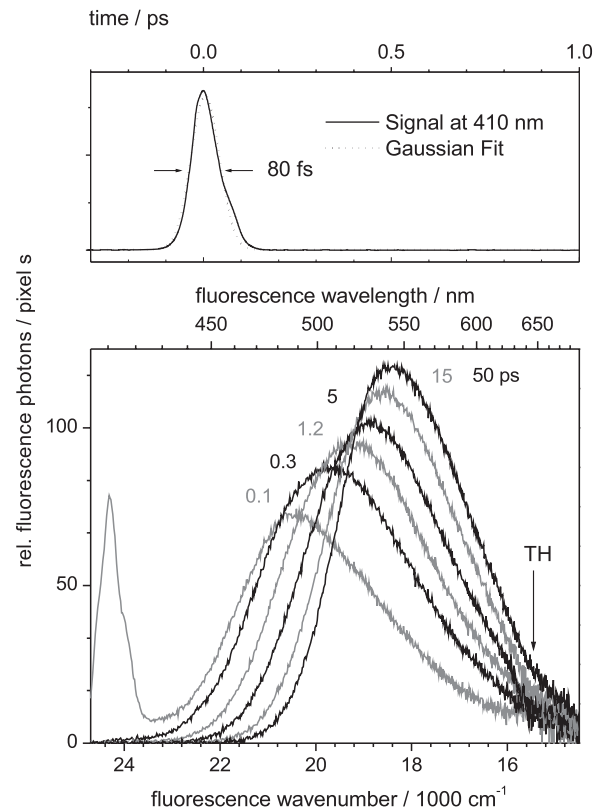


FIG. 10. Transient fluorescence spectra of C153 in methanol at 0.1, 0.3, 1.2, 5, 15, and 50 ps (*Bottom panel*). Shown are the relative quantum distributions over wavelength, i.e., after photometric and time corrections, for perpendicular polarization between gate pulse and fluorescence. The data were obtained by averaging over 16 scans. The sharp peak at blue side of the spectrum at 0.1 ps is the tail end of pump scatter. At TH, the third harmonic of the gate pulse rendered measurement impossible in previous designs.³⁴ *Top panel*: the time trace of residual pump scatter shows the instrument response function.

we measure the transient fluorescence of BBOT in methanol. The raw signal (λ_F, t) is shown as contour plot in Fig. 9, together with the time-zero function. With a time resolution of 80 fs, small changes of the vibronic fluorescence structure are observed before 200 fs. In the right panel the late raw signal (1 ps, black line) is compared to the fluorescence quantum distribution from stationary measurements (gray). Such comparisons were made above for photometric calibration. In the present case, the vibronic emission band of BBOT at 437 nm is reduced by the yellow glass filter.

IV. C153 IN METHANOL: A REFERENCE FOR TRANSIENT FLUORESCENCE BAND-SHAPE MEASUREMENTS

C153 has been studied extensively as a probe in time-resolved Stokes shift measurements^{9,17,34,37-40,43} and has become a standard in this field. Sets of scans were taken from negative delays up to 4 ps in 20 fs steps, to 40 ps in 200 fs steps, and to 100 ps in 500 fs steps. Transient upconverted spectra corrected for group velocity dispersion, and photometrically as discussed above, are shown in Fig. 10. Fluorescence polarized perpendicularly to the pump polarization is recorded in order to minimize contributions from Raman scattering of the solvent. As a consequence, the amplitude rises on the ps time scale due to electronic change and rotational diffusion of the emitting chromophore. We find biexponential behavior of the anisotropy decay, as in Ref. 52 but with faster initial component (0.3 ps, 38%). However, the fact that

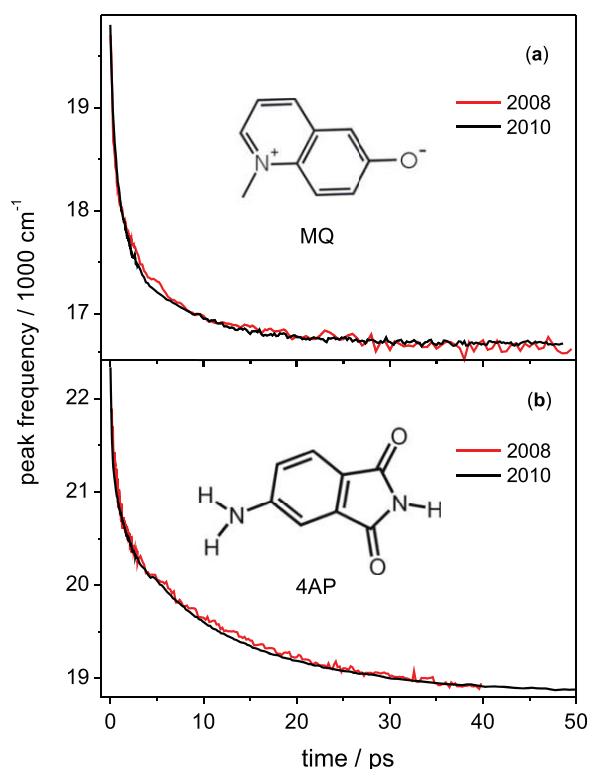


FIG. 11. (Color online) The reproducibility of the upconversion experiment is seen by measurements which were recorded two years apart. Shown is the peak frequency as function of time, for methyl quinolone (a)⁴⁹ and 4-amino phthalimide (b)⁵⁰ in methanol.

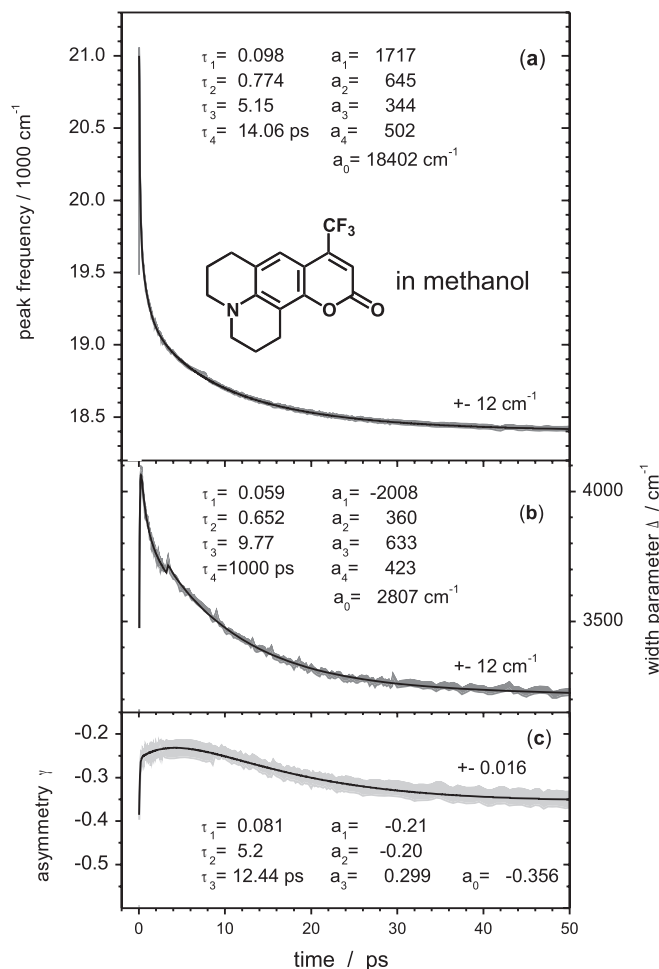


FIG. 12. Evolution of lognormal parameters (Eq. (2)) for the fluorescence distribution $f^{(F)}(\tilde{\nu}_F)$ from C153 in methanol. Gray bands outline the 95% confidence interval of the lognormal fits. For the time range 0.1–80 ps, the evolution is described by $\sum a_i \exp\{-t/\tau_i\} + a_0$ (black lines) with the parameters given as insets. A weak (2%) satellite pulse is responsible for a kink in (b) at 3.4 ps. The evolution of the average emission frequency can be derived.⁵¹

the amplitude rises does not influence the determination of the spectral position and band shape. The sharp peak near the blue edge of the spectrum at 100 fs is due to tailing pump scatter. After transformation to photon distributions over wavenumbers, the spectra are fitted with a lognormal function. Thus, for every delay time t , we obtain the fit parameters together with their standard error (SE), comprising the final result.

The reproducibility of dynamic fluorescence measurements with the new setup is demonstrated in Fig. 11. Here the evolution of peak frequency, in methanol, is shown for methyl quinolone (MQ, a) and for 4-amino phthalimide (4AP, b). The two measurements in each case were performed two years apart.

Let us return to C153 in methanol. Figure 12 shows the evolution of peak position $\tilde{\nu}_0(t)$, bandwidth parameter $\Delta(t)$, and asymmetry parameter $\gamma(t)$, in bands of $\pm 2SE$ for 95% confidence. Here the confidence interval refers to the lognormal fit only and may be subject to other experimental problems. For example, a weak satellite of the pump pulse is responsible for a sudden increase of bandwidth at 3.4 ps (panel b). This perturbation can be removed by data analysis. Note that a multiexponential temporal fit of $\tilde{\nu}_0(t)$ may

have different errors (slightly smaller in this case) because correlated changes over a large spectral range are measured. The Stokes shift from $t = 0.1$ ps to time-infinity is determined as 2020 cm^{-1} . This value is smaller than the total shift (2190 cm^{-1}) from our stationary estimates⁹ (see Fig. 2). We do not see the oscillations of $\tilde{\nu}(t)$ which were reported and analyzed recently.⁴⁰ Parameters for multiexponential fits (red lines) are given as insets. Such data could be used to develop this and other femtosecond fluorescence spectrometers consistently.⁵³

ACKNOWLEDGMENTS

X.-X.Z. is grateful for the support by the Chinese Scholarship Council. N.P.E. thanks the Deutsche Forschungsgemeinschaft (Grant No. ER 154/9–1).

- ¹H. Mahr and M. D. Hirsch, *Opt. Comm.* **13**, 96 (1975).
- ²M. A. Kahlow, W. Jarzeba, T. P. DuBruil, and P. F. Barbara, *Rev. Sci. Instrum.* **59**, 1098 (1988).
- ³W. Jarzeba, G. C. Walker, A. E. Johnson, M. A. Kahlow, and P. F. Barbara, *J. Phys. Chem.* **92**, 7039 (1988).
- ⁴D. C. Todd, J. M. Jean, S. J. Rosenthal, A. J. Ruggiero, D. Yang, and G. R. Fleming, *J. Chem. Phys.* **93**, 8658 (1990).
- ⁵R. Jimenez, G. R. Fleming, P. V. Kumar, and M. Maroncelli, *Nature (London)* **369**, 471 (1994).
- ⁶S. E. Bradforth, R. Jimenez, F. V. Mourik, R. V. Grondelle, and G. R. Fleming, *J. Phys. Chem.* **99**, 16179 (1995).
- ⁷B. P. Krueger, G. D. Scholes, R. Jimenez, and G. R. Fleming, *J. Phys. Chem. B* **102**, 2284 (1998).
- ⁸I. V. Rubtsov and K. Yoshihara, *J. Phys. Chem. A* **103**, 10202 (1999).
- ⁹M. L. Horng, J. A. Gardecki, A. Papazyan, and M. Maroncelli, *J. Phys. Chem.* **99**, 17311 (1995).
- ¹⁰D. Marks, P. Proposito, H. Zhang, and M. Glasbeek, *Chem. Phys. Lett.* **289**, 535 (1998).
- ¹¹M. Chatteraj, B. A. King, G. U. Bublitz, and S. G. Boxer, *Proc. Natl. Acad. Sci. U.S.A.* **93**, 8362 (1996).
- ¹²X. H. Shi, P. Abbyad, X. K. Shu, K. Kallio, P. Kanchanawong, W. Childs, S. J. Remington, and S. G. Boxer, *Biochemistry* **46**, 12014 (2007).
- ¹³S. Takeuchi and T. Tahara, *J. Phys. Chem. A* **102**, 7740 (1998).
- ¹⁴T. Fiebig, M. Chachisvillisi, M. Manger, A. H. Zewail, A. Douhal, I. Garcia-Ochoa, and A. D. L. H. Ayuso, *J. Phys. Chem. A* **103**, 7419 (1999).
- ¹⁵S. K. Pal, J. Peon, and A. H. Zewail, *Chem. Phys. Lett.* **363**, 57 (2002).
- ¹⁶S. K. Pal, L. Zhang, and A. H. Zewail, *Proc. Natl. Acad. Sci. U.S.A.* **100**, 8113 (2003).
- ¹⁷T. Gustavsson, L. Cassara, V. Gulbinas, G. Gurzadyan, J.-C. Mialocq, S. Pommeret, M. Sorgius, and P. V. D. Meulen, *J. Phys. Chem. A* **102**, 4229 (1998).
- ¹⁸T. Gustavsson, N. Sarkar, E. Lazzarotto, D. Markovitsi, and R. Improta, *Chem. Phys. Lett.* **429**, 551 (2006).
- ¹⁹H. S. Cho, H. Rhee, J. K. Song, C.-K. Min, M. Takase, N. Aratani, S. Cho, A. Osuka, T. Joo, and D. Kim, *J. Am. Chem. Soc.* **125**, 5849 (2003).
- ²⁰A. Fürstenberg, M. D. Julliard, T. G. Deligeorgiev, N. I. Gadjev, A. A. Vasilev, and E. Vauthey, *J. Am. Chem. Soc.* **128**, 7661 (2006).
- ²¹Y.-T. Kao, C. Saxena, T.-F. He, L. J. Guo, L. J. Wang, A. Sancar, and D. P. Zhong, *J. Am. Chem. Soc.* **130**, 13132 (2008).
- ²²L. Y. Zhang, Y. Yang, Y.-T. Kao, L. J. Wang, and D. P. Zhong, *J. Am. Chem. Soc.* **131**, 10677 (2009).
- ²³P.-T. Chou, Y.-C. Chen, W.-C. Chen, W.-S. Yu, Y.-H. Chou, C.-Y. Wei, and Y.-M. Cheng, *J. Phys. Chem. A* **105**, 1731 (2001).
- ²⁴C.-Y. Chen, C.-T. Cheng, J.-K. Yu, S.-C. Pu, Y.-M. Cheng, and P.-T. Chou, *J. Phys. Chem. B* **108**, 10687 (2004).
- ²⁵T. Pancur, N. K. Schwalb, F. Renth, and F. Temps, *Chem. Phys.* **313**, 199 (2005).
- ²⁶N. K. Schwalb and F. Temps, *Phys. Chem. Chem. Phys.* **8**, 5229 (2006).
- ²⁷G. Zgrablić, S. Haacke, and M. Chergui, *J. Phys. Chem. B* **113**, 4384 (2009).
- ²⁸D. V. O'Connor and D. Phillips, *Time-Correlated Single Photon Counting*, 1st ed. (Academic, London, 1984).
- ²⁹J. A. Gardecki and M. Maroncelli, *J. Phys. Chem. A* **103**, 1187 (1999).
- ³⁰T. Gustavsson, G. Baldecchino, J.-C. Mialocq, and S. Pommeret, *Chem. Phys. Lett.* **236**, 587 (1995).
- ³¹A. Cannizzo, O. Bräm, G. Zgrablic, A. Tortschanoff, A. Ajdarzadeh-Oskouei, F. van Mourik, and M. Chergui, *Opt. Lett.* **32**, 3555 (2007).
- ³²R. Schanz, S. A. Kovalenko, V. Kharlanov, and N. P. Ernsting, *Appl. Phys. Lett.* **79**, 566 (2001).
- ³³S. A. Kovalenko, R. Schanz, T. Senyushkina, and N. P. Ernsting, *Phys. Chem. Chem. Phys.* **4**, 703 (2002).
- ³⁴L. Zhao, J. L. Pérez-Lustres, V. Farztdinov, and N. P. Ernsting, *Phys. Chem. Chem. Phys.* **7**, 1716 (2005).
- ³⁵P. Fita, Y. Stepanenko, and C. Radzewicz, *Appl. Phys. Lett.* **86**, 021909 (2005).
- ³⁶X.-F. Han, X.-H. Chen, Y.-X. Weng, and J.-Y. Zhang, *J. Opt. Soc. Am. B* **24**, 1633 (2007).
- ³⁷P. Changenet-Barret, C. T. Choma, E. F. Gooding, W. F. DeGrado, and R. M. Hochstrasser, *J. Phys. Chem. B* **104**, 9322 (2000).
- ³⁸R. S. Fee and M. Maroncelli, *Chem. Phys.* **183**, 235 (1994).
- ³⁹S. J. Rosenthal, R. Jimenez, G. R. Fleming, P. V. Kumar, and M. Maroncelli, *J. Mol. Liq.* **60**, 25 (1994).
- ⁴⁰I. Eom and T. Joo, *J. Chem. Phys.* **131**, 244507 (2009).
- ⁴¹D. V. Matyushov and M. D. Newton, *J. Phys. Chem. A* **105**, 8516 (2001).
- ⁴²R. Improta, V. Barone, and F. Santoro, *J. Phys. Chem. B* **111**, 14080 (2007).
- ⁴³J. L. Perez-Lustres, F. Rodriguez-Prieto, M. Mosquera, T. A. Senyushkina, N. P. Ernsting, and S. A. Kovalenko, *J. Am. Chem. Soc.* **129**, 5408 (2007).
- ⁴⁴Y. Nabekawa and K. Midorikawa, *Opt. Express* **11**, 324 (2003).
- ⁴⁵N. P. Ernsting, J. Breffke, D. Y. Vorobyev, D. A. Duncan, and I. Pfeffer, *Phys. Chem. Chem. Phys.* **10**, 2043 (2008); U.S. and European patents pending DE 10 2006 039 425; U.S. Application patent 11/843,546.
- ⁴⁶M. Sajadi, A. L. Dobryakov, E. Garbin, N. P. Ernsting, and S. A. Kovalenko, *Chem. Phys. Lett.* **489**, 44(2010).
- ⁴⁷F. Zernike and J. E. Midwinter, *Applied Nonlinear Optics* (Wiley, New York, 1973).
- ⁴⁸*Lognormal Distributions: Theory and Applications*, edited by E. L. Crow and K. Shimizu, (Marcel Dekker, New York, 1988).
- ⁴⁹M. Sajadi, Y. Ajaj, I. Ioffe, H. Weingärtner, and N. P. Ernsting, *Angew. Chem. Int. Ed.* **49**, 454 (2009).
- ⁵⁰M. Sajadi, T. Obernhuber, S. A. Kovalenko, M. Mosquera, B. Dick, and N. P. Ernsting, *J. Phys. Chem. A* **113**, 44 (2008).
- ⁵¹From Eq. (3.11) of Ref. [9], a multiexponential fit of the average wavenumber curve so obtained gives $a_1 = 1546\text{ cm}^{-1}$, $\tau_1 = 0.091\text{ ps}$, $a_2 = 599\text{ cm}^{-1}$, $\tau_2 = 0.737\text{ ps}$, $a_3 = -164.3\text{ cm}^{-1}$, $\tau_3 = 21.9\text{ ps}$, $a_4 = 1132\text{ cm}^{-1}$, $\tau_4 = 14.6\text{ ps}$, and $a_0 = 17744\text{ cm}^{-1}$.
- ⁵²M. L. Horng, J. A. Gardecki, and M. Maroncelli, *J. Phys. Chem. A* **101**, 1030 (1997).
- ⁵³See supplementary material at <http://dx.doi.org/10.1063/1.3597674> for the absorption spectra of calibration dyes, details of gate energy determination, and parameters for solvation dynamic fits of C153 in methanol reported previously by other groups.